Journal of the Southeastern Association for Research in Astronomy, **7**, 45-50, 2012 December 1

MULTIBAND POLARIMETRY OF THE JET IN 3C 371

Riley P. Wetzel[1]
Department of Physics, Kalamazoo College, MI, 49006
and
Eric S. Perlman
Department of Physics and Space Sciences, Florida Institute of Technology, FL, 32901

ABSTRACT

We investigate the structure and dynamics of the relativistic jet emerging from the well known BL Lacertae (BL Lac) object known as 3C 371. The goal of this paper is to characterize the jet in 3C 371 and its polarization characteristics as a function of wavelength. We find several strong similarities between the C-band radio and the optical polarization data. Notably, the existence of a low polarization channel down the center of the jet was seen at radio wavelengths for the first time. As well, we find the low polarization channel in the radio image is wider, though apparently slightly shorter than its optical counterpart. These differences imply radio and optically emitting particle regions that are not exactly colocated. The similarities of the C-band radio and optical polarization data continue in the magnetic field position angle (MFPA) measurements. The MFPA measurements only appear to differ near the base of the low polarization channel, however, the significance is relatively low in that region in both bands. We also give estimates for the location of the major bend in the jet based on considerations of its polarimetric features. Finally, because of the low signal to noise ratio in our high energy radio data, we note the importance of obtaining higher resolution radio data for future observations.
Subject headings: galaxies, jets, polarization, magnetic field

1. INTRODUCTION

Relativistic jets are characterized as powerful, high speed, highly collimated outflows of plasma typically associated with a supermassive black hole (SMBH) at the center of an active galactic nucleus (AGN). Radio jets contain some of the most energetic particles anywhere in the Universe. The power of these outflows is immense and can be observed as different features on many angular scales. In some instances, jet emission can be observed on megaparsec scales. It is expected that the jets of AGN are powered by the aforementioned SMBH and transport energy, momentum, and angular momentum away from the AGN.

Though we continue to gain more knowledge of the emission processes of radio galaxies, a great deal of their underlying physics remain unclear. The composition of the jets is of particular interest today, and by studying the composition we wish to reveal more about the means of transporting energy within the jet. Further questions remain concerning the genesis near the SMBH, the dynamics of which are often difficult to observe due to the extreme luminosity of the core. Though many questions regarding these jets persist, scientists have made some significant progress and discoveries in recent years. The primary emission process for continuum sources from radio to optical UV frequencies is thought to be synchrotron in nature (Bridle & Perley 1984). In addition, scientists have learned that jets, in general (beyond extragalactic radio sources, and otherwise relativistic outflows), are the primary means of removing angular momentum from black hole accretion disks (Kuncic & Bicknell 2004).

The relativistic jet under examination in this paper emerges from the AGN known as 3C 371. 3C 371 is a well known BL Lac object, first classified as such by Miller (1975). It has a redshift of $z = 0.0508$ (Sandage 1967), which corresponds to a distance of approximately 223 Mpc making it is one of the nearest and brightest sources of its kind. The radio emission from 3C 371 was described as a 25" long, one-sided jet emerging to the west of the BL Lac (Wrobel & Lind 1990). Soon after, jet emission was seen in the optical regime via ground-based observations (Nilsson et al. 1997), and with the Hubble Space Telescope (HST) (Scarpa et al. 1999). Further observations of the jet, on milliarcsecond scales, showed a $1700:1$ jet to counter-jet flux ratio indicating a viewing angle of $\theta \lesssim 18^\circ$ (Gómez & Marscher 2000). Most recently, Sambruna et al. (2007) showed that synchrotron emission is the dominant emission mechanism from radio to x-ray frequencies for the jet in 3C 371.

In this paper we study 3C 371's jet using polarimetry. Polarimetry is one of the most powerful tools available to astronomers. An electromagnetic wave has three main characteristics: intensity, wavelength, and polarization. Most studies only take into account the first two, and indeed, the emission of many objects is unpolarized. A polarimetric study however, takes advantage of all three. This is indeed, a unique and powerful upside. Synchrotron radiation is expected to produce regions of highly polarized emission and polarimetry is intended to describe the structure and dynamics of magnetic fields in emission regions of distant objects. In regions of synchrotron emission, the degree of linear polarization indicates the ordering the of the magnetic field, while the implied MFPA vectors describe the orientation of the lo-

[1] Southeastern Association for Research in Astronomy (SARA) NSF-REU Summer Intern
Electronic address: riley.wetzel@gmail.com

cal magnetic field. Polarimetry in multiple bands can then reveal differences in the field geometry encountered by different radiation populations, which can then give a three-dimensional picture of the energetic and field structure in the jet. It is important to note, the orientation of the local B-field vectors, assumed to be 90° from the derived electric field vectors, may be affected by relativistic aberration in a relativistic flow (Lyutikov et al. 2005). Despite the immense power polarimetry offers, studies of this type remain relatively uncommon. This is largely because polarimetry is inherently difficult; it requires a very high signal-to-noise ratio but is a light starved process making high quality data difficult to obtain.

In this paper we discuss polarization features of 3C 371's jet as a function of wavelength. We also pay special attention to any sudden changes in MFPA throughout the jet as this can indicate perturbations in the jet possibly caused by the surrounding interstellar medium. Section 2 outlines relevant observations, and data reduction techniques. In Section 3, we present results of jet morphology as well as polarization characteristics in multiple bands. In Section 4 we discuss and summarize our findings.

2. DATA REDUCTION

2.1. *Observations and Processing*

We present VLA radio data observed in three radio bands: C-band ($\lambda \sim 6.2$ cm) observed on March 21, 1986, X-band ($\lambda \sim 3.6$ cm) observed on June 16, 2007, and K-band ($\lambda \sim 1.3$ cm) observed on July 21, 2002. Further, we present data from the optical band ($\lambda \sim 5910\mathring{A}$) observed with the HST. The HST observations were obtained with the Advanced Camera for Surveys (ACS) using the Wide Field Camera (WFC) and the POLV polarizer was used along with the F606W wide band filter. For a discussion of the reduction and mapping of the optical data see Perlman et al. (2006). We obtained the C-band and K-band radio data from Sambruna et al. (2007) and Cheung (2004).

The X-band data was obtained from the NRAO Data Archive System. 3C 371 was observed with the array in the A-configuration for intervals on the order of 30 seconds on average with several observations to maximize (u,v) coverage. It is important to note these observations occurred during the Expanded Very Large Array (EVLA)-VLA transition period meaning our data was gathered from a combination of 10 EVLA antennas and 17 VLA antennas. This transition from the old system to the EVLA, as described on the NRAO website, was implemented to improve the sensitivity of the array by a factor of at least 10. Before any processing could be done we had to flag all of the EVLA antennas out of our data. This was necessary because the EVLA and VLA receivers are very different, particularly in their bandpass and frequency specs. At the time, the polarization characteristics of the two receiver systems were very poorly known and therefore could not be accounted for via self-calibration or other standardized techniques. The draw back to removing 10 antennas, of course, is that our signal to noise ratio decreases. We then flagged further antennas using the AIPS task TVFLG on the basis of weak signals and one because it was offline during the observing period. All of our imaging and data processing was performed in AIPS. Standard AIPS tasks were employed to reduce the data set as outlined in the AIPS Cookbook (Greisen et al. 2006). The source 1331+305 was used as the primary flux density calibrator throughout our reduction.

2.2. *Imaging*

In this paper we discuss many of our images in terms of the Stokes parameters. There are four Stokes parameters that can be used to completely describe the polarization state of an electromagnetic wave. The first Stokes parameter is I, it simply describes the intensity of a light wave. The Stokes Q and U parameters describe a wave's linear polarization. A positive Stokes Q parameter corresponds to a horizontal plane-polarization state, while a negative corresponds to a vertical one. Positive and negative Stokes U parameters indicate a plane-polarization state at ±45°, respectively. There is a fourth Stokes parameter, V, that describes circular polarization, but we have no need for it in what follows.

We ran cycles of cleaning and self-calibration using the AIPS task SCIMG. We solved only for phase solutions in the first runs and then included solutions for amplitude and phase to produce our total intensity Stokes I map. Finally, we created Stokes Q and U maps using the task IMAGR in AIPS while maintaining the same clean component regions as for the Stokes I map. It was then straight forward to create images of the linearly polarized intensity, P, linear polarization position angle, MFPA, and fractional linear polarization, $FPOL$. Using the AIPS task COMB we created the aforementioned maps based on the following equations:

$$P = \sqrt{I_Q^2 + I_U^2}, \tag{1}$$

$$MFPA = \frac{1}{2}\arctan\left(\frac{I_U}{I_Q}\right) + 90°, \tag{2}$$

$$FPOL = \frac{P}{I}. \tag{3}$$

In each case the maps were clipped to specify a minimum signal to noise level of 3σ. We also remapped these same three images for the C-band and K-band data in order to display data with the same minimum significance. In order to constrain the uncertainties in our data, we created error maps for P and MFPA using the AIPS task COMB for all three radio bands based on the rms noise in the Stokes Q and U images. We further calculated errors from the Stokes Q and U maps on their own and summed them in quadrature to check the accuracy of our measurements.

2.3. *Uncertainties*

It is important to note that the optical data has some differences in terms of how it was processed. As described in the ACS Data Handbook, there is a small instrumental polarization intrinsic with the HST setup used for our optical observations of about 2.1%. These errors were added in quadrature with the errors from the Stokes Q and U maps to constrain the fractional polarization error estimates. In addition, point source subtraction was performed on the optical image prior to any other analysis. This method, described in detail in Perlman et al. (2006),

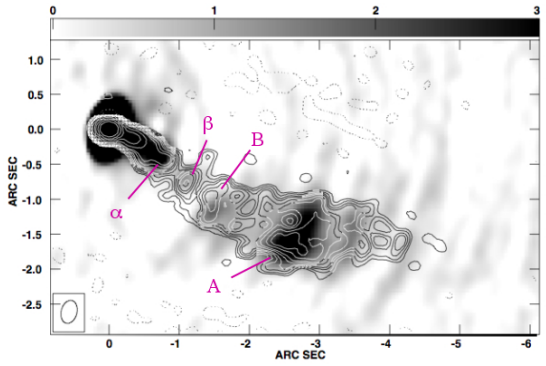

FIG. 1.— Seen here is a grey scale image of the X-band Stokes I image overlaid with contours of 1.35 GHz MERLIN Stokes I image resampled to geometry of X-band image using the AIPS task OHGEO. The cores have been registered to the same center, though the beams were not convolved. The labels indicate the knot nomenclature as defined by Sambruna et al. (2007). The contour levels are 0.1 × (-5,5,8,12,16,24,32,48,64,128,256,512,1024,2048) mJy beam^{-1}.

used a quadranted model that also assumed the source to be circularly symmetric. This yields possible uncertainty in core registration. Unfortunately due to further processing differences, we are, as yet, unable to provide uncertainty measurements on the optical MFPA data. Instead, because the images were processed in the same way, we will assume errors for the optical data consistent with Perlman et al. (2006). In general, the uncertainties for optical polarization are ±5%, and the uncertainties in MFPA will be assumed to be ±10°. For the remainder of the paper, we will quote specific uncertainties as necessary.

3. RESULTS

Prior to any image comparisons, we registered the cores of our images to the coordinates of the data with the highest resolution, the peak of the X-band data (at RA = $18^h06^m50.^s681$, Dec. = 69°49′28″.108 in J2000). This provided us with the most accurate absolute astrometry.

3.1. *Jet Morphology*

The optically visible portion of the jet in 3C 371 has four main knots. Figure 1 shows a high resolution image of the X-band Stokes I image in grey-scale overlaid with total intensity contours from a 1.35 GHz MERLIN image obtained from Sambruna et al. (2007). The knots have been labelled according to the nomenclature of Sambruna et al. (2007) (note that this is different from the labels used in Perlman et al. (2006)). In Figures 2-5, it is possible to see the same knot structures at all four wavelengths. Note well, the extended feature directly to the west of the origin in the optical image is a diffraction spike and should not be considered part of the emission region. We have been unable to detect any significant positional offsets in the knot locations between bands. Well-matched optical and radio morphologies in 3C 371 have been found before (e.g. Sambruna et al. (2007)).

The overall morphology of the jet can be described by an initial outflow toward the south-west of the origin with an apparent bend in the jet after which the flow appears directly to the west. The jet also appears to widen near the region of knot A. The nature of the bend is subtle and so it becomes difficult to localize. Rough visual estimates place the location of the bend between 2.0″ and 3.0″ from the nucleus. In the high resolution MERLIN image of Figure 1, there may be evidence for a smaller bend immediately to the west of the nucleus in addition to the larger bend further downstream.

Significant jet emission appears in the C-band radio image up to ∼ 5.0″ downstream of the core, and exhibits a large width of ∼ 1.5″ throughout the length. Conversely, significant optical emission of 3C 371 begins to fade only ∼ 3.5″ downstream of the nucleus. Profiles of the X-band and K-band images exhibit emission to similar distances as the optical image, but also have much skinnier emission regions throughout their lengths as compared to the C-band radio image.

3.2. *Jet Polarimetry*

At this point in our study, the significance of the results throughout the majority of the emission region in the X-band and K-band data was too low for us to trust in comparison with the optical and C-band radio data. In addition, and this could be a point for further investigation because, particularly in the case of the X-band map (Figure 3), the polarization vectors do not agree with the highly significant C-band data in regions where they overlap. Due to the lack of highly significant polarization data available in the X-band and K-band radio data, our polarimetry analysis will primarily cover results of only the C-band radio data and the optical data of 3C 371.

The polarization vectors rotated through 90° in Figures 2 and 5 show the magnetic field structure in the emission regions of the C-band and optical data, respectively. Note well, the polarization vectors may not show the true projected B-field structure as they may be altered by relativistic aberration as discussed in section 1. The MFPA throughout the C-band image is almost exclusively parallel to the jet axis. The optical MFPA exhibits several areas in strong agreement with the C-band radio data. In the southern lobe of knot A the radio MFPA (measured north through east) is ∼ 76 ± 1° and the optical MFPA is ∼ 75° ± 10° (recall that we are assuming optical errors from Perlman et al. (2006)). In the northern lobe of the same knot the structure the vectors are slightly rotated. The C-band MFPA is ∼ 63±1° while the optical is ∼ 59° ± 10° in the same region. However there are some differences between the two wavelengths. Closer to the nucleus and near the jet axis, the MFPA in the C-band data remains parallel to the jet axis, while the optical data exhibits a nearly 90° degree rotation. It is important to note, however, that the results in this region are detected with relatively low significance.

A striking polarimetric feature of the optical jet in 3C 371 first noted by Perlman et al. (2006) is the presence of a low-polarization 'channel' extending down the center of the jet for most of its length. Originally, this feature was only noted at optical wavelengths and can be seen in Figure 6. Now, as seen in Figure 7, a similar region of low polarization extends down the center of the jet in the C-band radio image. The channel is present over roughly the same distance in both bands, $\gtrsim 2.0''$, with perhaps a slightly longer channel in the optical image. The low polarization channel reaches a maximum width of ∼ 0.9″ in the C-band, but only ∼ 0.6″ in the optical image. Again, compared to other regions in the jet, it is important to note that the low polarization channel is detected with relatively low significance. The fact

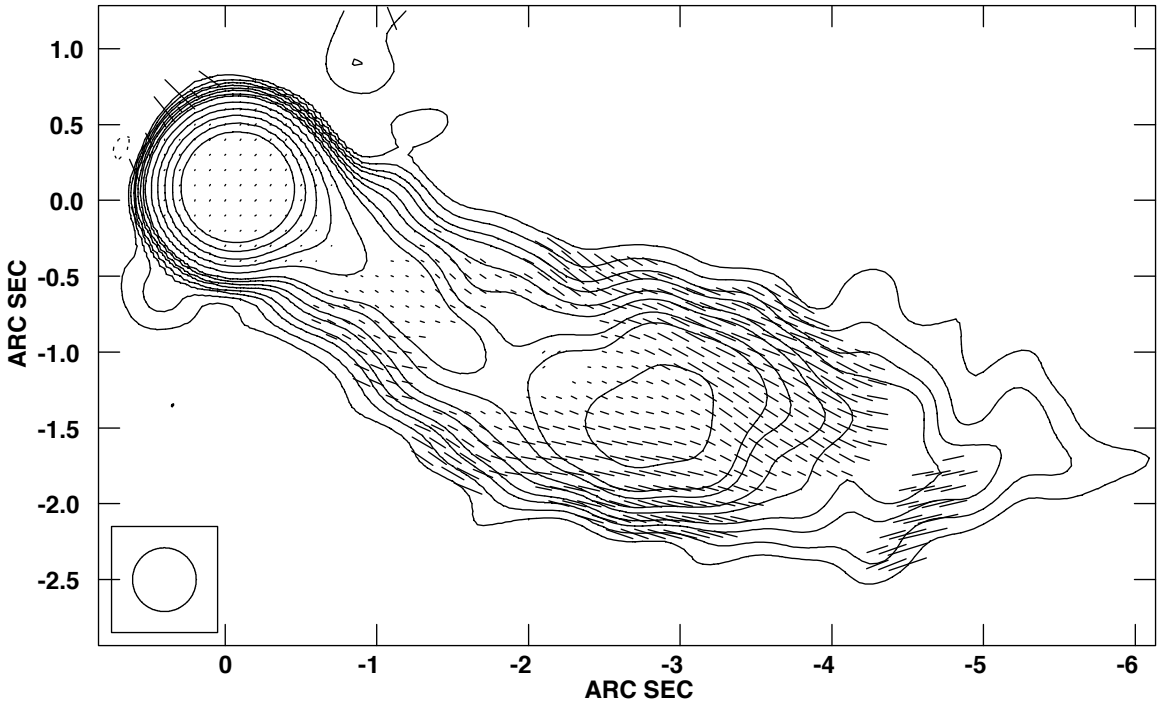

FIG. 2.— Polarization map of C-band radio data. Contours represent Stokes I intensity. The contour levels are 0.1 × (-5,5,8,12,16,24,32,48,64,128,256,512,1024,2048) mJy beam^{-1}. A vector 1″ long corresponds to 290% polarization.

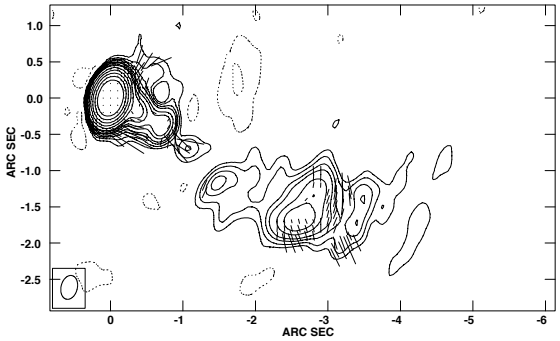

FIG. 3.— Polarization map of X-band radio data. Contours represent Stokes I intensity. The contour levels are 0.1 × (-5,5,8,12,16,24,32,48,64,128,256,512,1024,2048) mJy beam^{-1}. A vector 1″ long corresponds to 290% polarization.

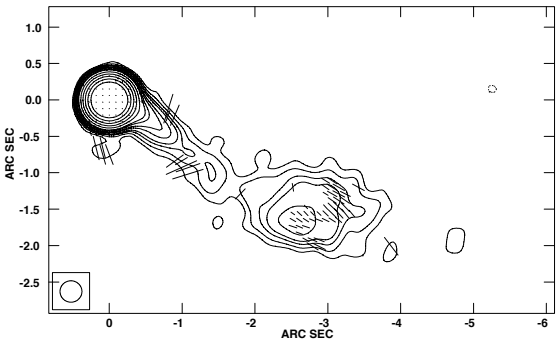

FIG. 4.— Polarization map of K-band radio data. Contours represent Stokes I intensity. The contour levels are 0.1 × (-5,5,8,12,16,24,32,48,64,128,256,512,1024,2048) mJy beam^{-1}. A vector 1″ long corresponds to 290% polarization.

that the low polarization channels vary in size between the two frequencies implies that the optically and radio emitting particle populations are not exactly colocated. See Perlman et al. (1999) for a more in depth discussion of non-colocated emitting populations.

Another feature first noted in the optical observations of Perlman et al. (2006) is the presence of high polarization regions near the jet edges. Both the C-band radio and optical images show regions of monotonically increasing polarization toward the edges near knot A. These regions in the radio band are detected at a significance of $\sim 30\sigma$, and in the optical at $\sim 20 - 25\sigma$. In the C-band the jet approaches almost 60 percent polarization in the northern edge of knot A and 45 percent polarization in the southern edge of knot A. The optical fractional polarization increases to greater than 30 percent in the northern edge of the same knot, and to about 40 percent in the south.

4. DISCUSSION AND SUMMARY

Studies of 3C 371 have become more numerous over the past few decades, however studies of the jet associated with the BL Lac object, especially in multiple bands, remain uncommon. Keeping in mind the small number of polarimetric studies underway today, this paper is one of very few to discuss polarimetry of 3C 371's jet with an eye toward multi-wavelength features. Perlman et al. (2006) was one of the first to do a polarimetric study in the optical, while Sambruna et al. (2007) is one of the only to have presented a polarimetric study of this object in multiple bands.

We have presented polarimetry data of the relativistic jet associated with the BL Lac object 3C 371. Multiband polarimetric studies can provide unique looks at the magnetic fields of astronomical sources. This type of study was particularly useful to us due to the synchrotron nature of the jet emission in this paper.

Reasons for the large bend in the jet's direction of propagation are still highly unknown, but our data provide several possible avenues to explore this dynamic. A first step to understanding more about the bend would

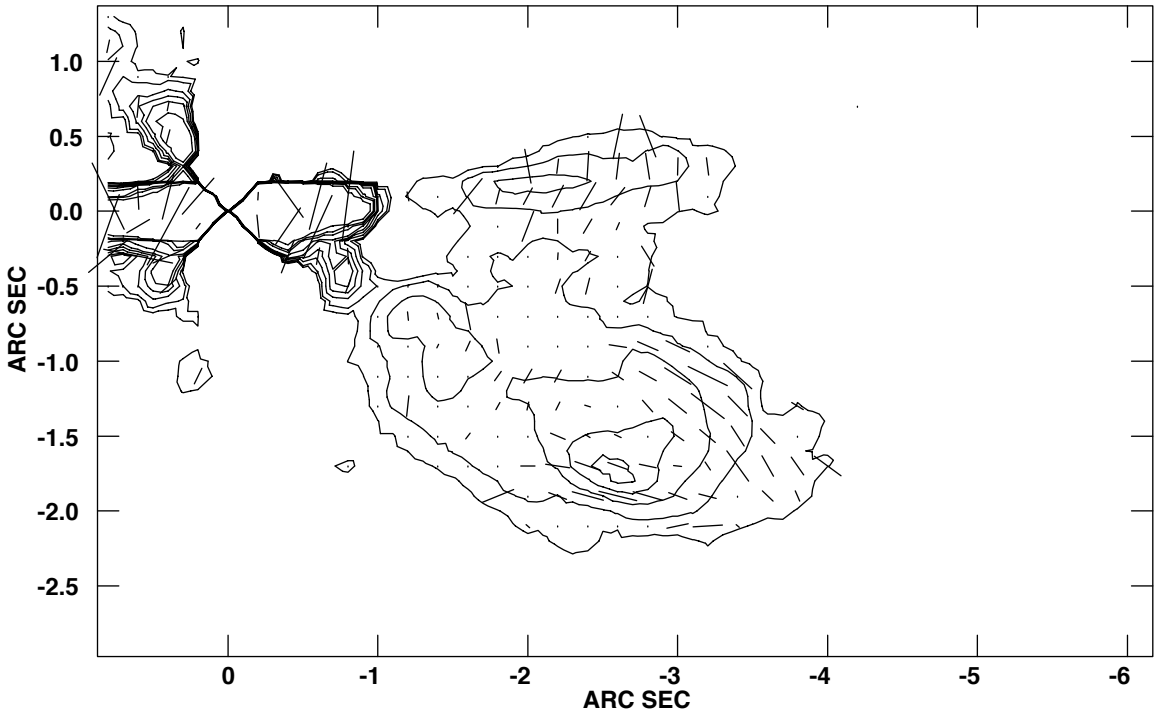

FIG. 5.— Polarization map of optical data. The electric vectors have been rotated by 90° as to indicate the apparent local B-field.

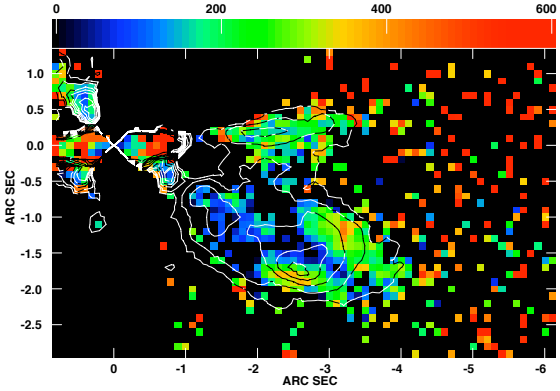

FIG. 6.— Fractional polarization of the optical data. Contours represent Stokes I intensity, while the color scale indicates the percentage of polarized flux according to the scale along the top.

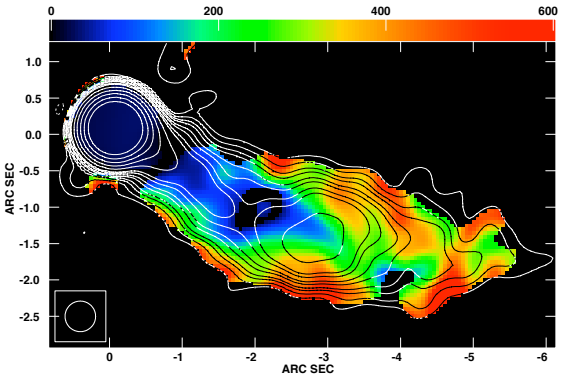

FIG. 7.— Fractional polarization of the C-band radio data. Contours represent Stokes I intensity, while the color scale indicates the percentage of polarized flux according to the scale along the top.

be to constrain it. Regions of increasing, high edge-polarization, as described in Section 3.2, near the northern and southern edges of knot A, in which the polarization vectors also follow the flux contours, as seen in the C-band data, can be indicative of shearing along the edge of the jet (Perlman et al. 2006). This trend has been seen in other jets near bends and could indicate an interaction of the jet's local magnetic field and the surrounding interstellar medium (ISM). In other words, the regions of high edge-polarization could correspond to the location of the jet bend. Another avenue to examine is to look for sudden changes in the MFPA of the jet as this could be a result of perturbations in the jet flow. The polarization vectors in the C-band show first signs of rotation $\sim 3.0''$ from the nucleus, which could be another indicator of the site of the jet bend.

The HST data as well as the C-band VLA data we present in this paper show several similarities in terms of polarization features that were not noted before in both bands. Most notably, we see the low polarization channel in the radio regime for the first time. As mentioned in section 3.2, these channels are not entirely colocated in the two bands and this serves as evidence that optical and radio emission originates in somewhat different physical regions. Unfortunately the VLA data for the X-band and K-band images did not yield highly significant polarization information throughout the majority of the jet and as a result we were not able to trust the data for use in our study. Reobserving this jet in the X-band and the K-band regimes using the more sensitive and higher resolution EVLA array could prove highly valuable in completing a picture of the jet's polarization characteristics with respect to wavelength. The increased sensitivity would allow for better constraints on polarization measurements, and hopefully be able to explain some of the major differences we see in the MFPA measurements of

the different radio bands.

We showed images of the jet with polarization characteristics in three radio bands, and one optical. We found that the morphology of the jet in the optical and radio did not differ significantly. The optical data and C-band VLA data showed several strong similarities in polarization patterns as well as MFPA characteristics. Due partly to insufficient data, and partly to time constraints, our initial goal of creating a description of the polarization characteristics of 3C 371's jet as a function of wavelength is not yet complete. We hope to further constrain error measurements in the optical data and bring together a more comprehensive description of the polarization characteristics of this jet.

More work in the future will be necessary to begin to uncover some of the little known dynamics of these jets. Completion of this study could be a big step in the right direction. Continued research of this object could help to unlock some of the more mysterious questions surrounding extragalactic sources of emission of all kinds.

This project was funded by the National Science Foundation Research Experiences for Undergraduates (REU) program through grant NSF AST-1004872.

REFERENCES

Bridle, A. H., & Perley, R. A. 1984, ARA&A, 22, 319
Cheung, C. C. 2004, Ph.D. Thesis,
Gómez, J.-L., & Marscher, A. P. 2000, ApJ, 530, 245
Greisen, E. et al. 2006, AIPS Cookbook, http://www.aips.nrao.edu/cook.html
Lyutikov, M., Pariev, V. I., & Gabuzda, D. C. 2005, MNRAS, 360, 869
Kuncic, Z., & Bicknell, G. V. 2004, ApJ, 616, 669
Miller, J.S. 1975, ApJ, 200, L55
Nilsson, K., Heidt, J., Pursimo, T., Silanpää, A., Takalo, L. O., & Jaeger, K. 1997, ApJ, 484, L107
Perlman, E. S., Biretta, J. A., Zhou, F., Sparks, W. B., & Macchetto, F. D. 1999, AJ, 117, 2185
Perlman, E. S., Padgett, C. A., Georganopoulos, M., et al. 2006, ApJ, 651, 735
Pesce, J. E., Sambruna, R. M., Tavecchio, F., Maraschi, L., Cheung, C. C., Urry, C. M., & Scarpa, R. 2001, ApJ, 556, L79
Sambruna, R. M., Donato, D., Tavecchio, F., et al. 2007, ApJ, 670, 74
Sandage, A. 1967, ApJ, 150, L9
Scarpa, R., Urry, C. M., Falomo, R., & Treves, A. 1999, ApJ, 526, 643
Wrobel, J.M., & Lind, K.R. 1990, ApJ, 348, 135